INTERNATIONAL JOURNAL FOR NUMERICAL METHODS IN FLUIDS VOL. 21, 35–48 (1995)

A NUMERICAL MODELLING STUDY OF THE FLOW AND SALINITY STRUCTURE IN THE GODAVARI ESTUARY, EAST COAST OF INDIA

A. D. RAO

Centre for Atmospheric Sciences, Indian Institute of Technology, Delhi, Hauz Khas, New Delhi 110016, India

SUMMARY

The Godavari Estuary in Andhra Pradesh (a state bordering the east coast of India) communicates with the Bay of Bengal. Conditions in the estuary are characterized by a seasonally varying freshwater discharge and an intrusion of salt water from the bay dependent upon the flow associated with the semi-diurnal component of the astronomical tide. A numerical model is applied to simulate the flow and salinity structures, which in the case of the Godavari Estuary have also been determined observationally and are documented in the literature. Observational data on the flow and salinity structure during two seasons are used in a comparison with theoretical results derived using a turbulent energy equation. Reasonable agreement is obtained between the model results and the observational data; in particular, streamlines are computed for the tidally averaged (or mean) component of the density-controlled flow.

KEY WORDS numerical modelling; estuarian circulation; turbulence energy; salinity structure; Bay of Bengal; tidal wave

INTRODUCTION

The extent of the landward intrusion of saline water into a river estuary has a marked effect on the agricultural activity of adjacent land. Thus the distance of inland penetration may be expected to vary both seasonally and during the spring–neap tidal cycle. Because of this practical relevance, the development and application of a suitable numerical model are essential. The dynamical processes involving the interaction between river discharge and tidal currents are complex and lead to a series of distinctive types of estuary circulation. An account of these is given by Dyer[1] and Officer.[2] In this case the boundary between the fresh and saline water is sharp and well defined, with an almost total lack of mixing between the two layers. In the work presented here we have carried out simulations of the combined freshwater and tidal flow in the Godavari Estuary during the months of July and January and have compared these with observational data.[3]

FORMULATION OF THE MODEL

The origin O of a system of rectangular Cartesian co-ordinates is situated at the equilibrium level of the free surface of the water in the estuary. Ox points seaward from the landward end of the model estuary at $x = 0$; the seaward end is denoted by $x = L$ and Oz is measured vertically upward from $z = 0$. The displaced position of the free surface at time t is located at $z = \zeta(x, t)$ and the position of the bed of the estuary is at $z = -h(x)$. The breadth of the estuary at position x is dentoed by $b(x)$. The Reynolds-averaged components of velocity and fluid density are denoted by (u, w) and ρ respectively, the latter

CCC 0271–2091/95/010035–14

Received May 1994
Revised November 1994

being determined by the local values of the temperature T and the salinity S. The equation expressing the horizontal momentum balance in the model estuary then has the form

$$\frac{\partial}{\partial t}(bu) + \frac{\partial}{\partial x}(bu^2) + \frac{\partial}{\partial z}(buw) = -gb\frac{\partial \zeta}{\partial x} - \frac{b}{\rho}\int_z^\zeta \frac{\partial}{\partial x}(g\rho)\,dz + \frac{\partial}{\partial z}\left(K_M \frac{\partial}{\partial z}(bu)\right), \tag{1}$$

where ρ_0 is a constant reference density and K_M is a diffusion coefficient for vertical momentum exchange by turbulent processes.

The equation of continuity may be written in either of the equivalent forms

$$\frac{\partial}{\partial x}(bu) + \frac{\partial}{\partial z}(bw) = 0, \tag{2}$$

$$b\frac{\partial H}{\partial t} + \frac{\partial}{\partial x}(bH\bar{u}) = 0, \tag{3}$$

where H is the total depth $\zeta + h$ and $\bar{u}$ is the depth-averaged velocity given by

$$\bar{u} = \frac{1}{H}\int_{-h}^{\zeta} u\,dz. \tag{4}$$

The density is related to the local temperature and salinity by a linear equation of state in which

$$\rho = \rho_0(1 - \alpha T + \delta S), \tag{5}$$

where the constants α and δ have the respective values $2{\cdot}0 \times 10^{-4}\ ^\circ\mathrm{C}^{-1}$ and $7{\cdot}5 \times 10^{-4}\ \mathrm{ppt}^{-1}$.

The temperature and salinity are determined from transport equations of the form

$$\frac{\partial}{\partial t}(bT) + \frac{\partial}{\partial x}(buT) + \frac{\partial}{\partial z}(bwT) = \frac{\partial}{\partial z}\left(K_T \frac{\partial}{\partial z}(bT)\right), \tag{6}$$

$$\frac{\partial}{\partial t}(bS) + \frac{\partial}{\partial x}(buS) + \frac{\partial}{\partial z}(bwS) = \frac{\partial}{\partial z}\left(K_S \frac{\partial}{\partial z}(bS)\right), \tag{7}$$

where K_T and K_S are diffusion coefficients for thermal and salinity exchange respectively.

The parametrization of the turbulent processes is completed by the application of a transport equation for the Reynolds-averaged turbulence energy density E. This has the form

$$\frac{\partial}{\partial t}(bE) + \frac{\partial}{\partial x}(buE) + \frac{\partial}{\partial z}(bwE) = bK_M\left(\frac{\partial u}{\partial z}\right)^2 + \frac{g}{\rho_0}bK_D\frac{\partial \rho}{\partial z} + \frac{\partial}{\partial z}\left(K_E\frac{\partial}{\partial z}(bE)\right) - b\varepsilon, \tag{8}$$

where K_D and K_E are diffusion coefficients for vertical exchange of density and turbulence energy respectively.[4] Boundary conditions to accompany equation (8) lead to

$$\frac{\partial E}{\partial z} = 0 \quad \text{at } z = -h \text{ and } z = \zeta. \tag{9}$$

In the present work we prescribe that the diffusion coefficients are equal in value for all transfer processes, i.e.

$$K_M = K_T = K_S = K_D = K_E = K, \tag{10}$$

and, as used by Johns,[4] write

$$K = c^{1/4}lE^{1/2}, \qquad \varepsilon = \frac{c^{3/4}E^{3/2}}{l_D} \tag{11}$$

where l is a mixing length scale, l_D is a dissipation length scale and c is an empirical constant. The form used for the length scales is a unique feature of the present work and has been chosen to as to yield the best overall fit with the observational data reported by Rao *et al.*[3]

A basic length scale l_0 is defined by

$$l_0 = k(z + h + z_0) \exp\left[-\left(\frac{z+h}{H}\right)^{\gamma}\right], \tag{12}$$

where k and z_0 are von Karman's constant and the roughness length of bottom elements respectively. In terms of this we write

$$l = l_0 \exp\left[-\frac{1}{4}\beta\left(\frac{h_0}{h}\right)^2\left(\frac{z+h}{H}\right)\right], \tag{13}$$

where β and γ are constants and h_0 is a constant reference depth; thus, as $z \to -h$, $l \to kz_0$. A dissipation length scale l_D is defined by

$$l_D = l_0 \exp\left[\frac{3}{4}\beta\left(\frac{h_0}{h}\right)^2\left(\frac{z+h}{H}\right)\right]. \tag{14}$$

The dissipation term in equation (8) is parametrized by writing

$$\varepsilon = \frac{\varepsilon^{3/4}E^{3/2}}{l_D}. \tag{15}$$

At the floor of the estuary we apply a no-slip condition and take

$$u = 0 \quad \text{at } z = -h. \tag{16}$$

We prescribe zero applied surface wind stress and accordingly take

$$\frac{\partial u}{\partial z} = 0 \quad \text{at } z = \zeta. \tag{17}$$

Thus the fluid motion in the estuary is driven solely by boundary forcing applied at both ends of the estuary.

In the present study, however, we use a boundary condition at $x = 0$ (landward end of the estuary) that is compatible with there being a freshwater discharge through the model estuary. This may be achieved by prescribing that

$$\bar{u} + \left(\frac{g}{h}\right)^{1/2}\zeta = 2u_0 \quad \text{at } x = 0, \tag{18}$$

where u_0 is a constant velocity that determines the strength of the freshwater flow. Equation (18) is a crucial condition in the present modelling study, as its application implies that the tidal response in the estuary, which originates in the Bay of Bengal, passes freely through $x = 0$ in the form of a progressive wave and is not reflected by any upstream tidal barrier. At $x = L$ (seaward end of the estuary) a boundary condition is required that supports the semi-diurnal tide in the estuary. This is prescribed in the form

$$\bar{u} - \left(\frac{g}{h}\right)^{1/2}\zeta = -2u_L \sin(\sigma t) \quad \text{at } x = L, \tag{19}$$

where u_L is a constant velocity, the values of which will be chosen so as to produce the correct amplitude for the semi-diurnal tide; σ is the corresponding radian frequency (taken as $1{\cdot}405 \times 10^{-4}$ s^{-1}).

The boundary conditions for salinity and temperature during inflow and outflow are given by

$$\begin{aligned} &S = S_0 \text{ and } T = T_0 \quad \text{at } x = 0, \quad \text{where } u > 0, \\ &S = S_L \text{ and } T = T_L \quad \text{at } x = L, \quad \text{where } u < 0. \end{aligned} \tag{20}$$

Further conditions to accompany equations (6) and (7) require that

$$\frac{\partial T}{\partial z} = 0 \text{ and } \frac{\partial S}{\partial z} = 0 \quad \text{at } z = -h \text{ and } z = \zeta. \tag{21}$$

CO-ORDINATE TRANSFORMATION

A transformation of the vertical co-ordinate into a new non-dimensional vertical co-ordinate σ is introduced to facilitate the representation of the boundary conditions accurately at both the sea surface and the sea floor. This has the form

$$\sigma = \frac{z + h}{H}. \tag{22}$$

Thus σ increases monotonically from $\sigma = 0$ at the sea floor, $z = -h(x)$ to $\sigma = 1$ at the sea surface, $z = \zeta(x, t)$. The vertical velocity in the σ-co-ordinate, defined by

$$\omega = \frac{\mathrm{D}\sigma}{\mathrm{D}t} = \frac{\partial \sigma}{\partial t} + u\frac{\partial \sigma}{\partial x} + w\frac{\partial \sigma}{\partial z}, \tag{23}$$

is zero at both the sea floor and the sea surface. The new prognostic variables are defined by

$$\tilde{U} = bHu \qquad \tilde{S} = bHS, \qquad \tilde{T} = bHT, \qquad \tilde{E} = bHE. \tag{24}$$

Using x, σ and t as new independent variables and substituting for ρ from equation (1) leads to

$$\begin{aligned} \frac{\partial \tilde{u}}{\partial t} + \frac{\partial}{\partial x}(u\tilde{u}) + \frac{\partial}{\partial \sigma}(\omega\tilde{u}) = &- gbH\frac{\partial \zeta}{\partial x} + g\alpha bH^2\int_\sigma^1 \frac{\partial T}{\partial x}\,\mathrm{d}\sigma \\ &- g\alpha bH\left[\left((1-\sigma)T - \int_\sigma^1 T\,\mathrm{d}\sigma\right)\frac{\partial h}{\partial x} - \left(T_{\sigma=1} - \sigma T - \int_\sigma^1 T\,\mathrm{d}\sigma\right)\frac{\partial \zeta}{\partial x}\right] \\ &- g\delta bH^2\int_\sigma^1 \frac{\partial S}{\partial x}\,\mathrm{d}\sigma + g\delta bH \\ &\times\left[\left((1-\sigma)S - \int_\sigma^1 S\,\mathrm{d}\sigma\right)\frac{\partial h}{\partial x} + \left(S_{\sigma=1} - \sigma S - \int_\sigma^1 S\,\mathrm{d}\sigma\right)\frac{\partial \zeta}{\partial x}\right] \\ &+ \frac{1}{H^2}\frac{\partial}{\partial \sigma}\left(K\frac{\partial \tilde{u}}{\partial \sigma}\right). \end{aligned} \tag{25}$$

Transformation of equation (2) leads to a purely diagnostic equation for ω in which

$$\frac{\partial}{\partial x}\left[bH(u - \bar{u})\right] + \frac{\partial}{\partial \sigma}(bH\omega) = 0, \tag{26}$$

where $\omega = 0$ at $\sigma = 0$ and $\sigma = 1$. Equations (6) and (7) lead to

$$\frac{\partial \tilde{T}}{\partial t} + \frac{\partial}{\partial x}(u\tilde{T}) + \frac{\partial}{\partial \sigma}(\omega \tilde{T}) = \frac{1}{H^2}\frac{\partial}{\partial \sigma}\left(K\frac{\partial \tilde{T}}{\partial \sigma}\right), \tag{27}$$

$$\frac{\partial \tilde{S}}{\partial t} + \frac{\partial}{\partial x}(u\tilde{S}) + \frac{\partial}{\partial \sigma}(\omega \tilde{S}) = \frac{1}{H^2}\frac{\partial}{\partial \sigma}\left(K\frac{\partial \tilde{S}}{\partial \sigma}\right). \tag{28}$$

Likewise equation (8) becomes

$$\frac{\partial \tilde{E}}{\partial t} + \frac{\partial}{\partial x}(u\tilde{E}) + \frac{\partial}{\partial \sigma}(\omega \tilde{E}) = \frac{bK}{H^3}\left(\frac{\partial \tilde{u}}{\partial \sigma}\right)^2 - gb\alpha K\frac{\partial T}{\partial \sigma} + gb\delta K\frac{\partial S}{\partial \sigma} + \frac{1}{H^2}\frac{\partial}{\partial \sigma}\left(K\frac{\partial \tilde{E}}{\partial \sigma}\right) - bh\varepsilon. \tag{29}$$

The boundary conditions to accompany the set of transformed equations are now conveniently expressed at either $\sigma = 0$ or $\sigma = 1$. Equations (16) and (17) lead to

$$u = 0 \quad \text{at } \sigma = 0, \qquad \frac{\partial u}{\partial \sigma} = 0 \quad \text{at } \sigma = 1, \tag{30}$$

whereas equations (9) and (21) are equivalent to

$$\frac{\partial E}{\partial \sigma} = 0, \quad \frac{\partial T}{\partial \sigma} = 0 \text{ and } \frac{\partial S}{\partial \sigma} = 0 \quad \text{at } \sigma = 0 \text{ and } \sigma = 1. \tag{31}$$

The depth-averaged velocity $\bar{u}$ is now given by $\bar{u} = \int_0^1 u\,d\sigma$.

METHOD OF NUMERICAL SOLUTION

The equation described in the earlier section will be solved on a finite difference grid in the $x - \sigma$ domain. We define

$$\begin{aligned} x &= (i-1)\Delta x, \quad i = 1, 2, \ldots, m, & \Delta x &= L/(m-1), \\ \sigma &= (j-1)\Delta \sigma, \quad j = 1, 2, \ldots, n, & \Delta \sigma &= 1/(n-1). \end{aligned} \tag{32}$$

A discrete sequence of time instants is defined by

$$t = p\Delta t, \quad p = 0, 1, 2, \ldots. \tag{33}$$

Computations are carried out on a horizontally staggered grid for which two distinct types of computational points are defined.

The first of these, at odd points, are called ζ-points, at which ζ, ω, S and T are computed. Those at even points are u-points, at which u and E are computed. We choose m to be odd so that the end points of the computationsl domain correspond to ζ-points. An unstaggered grid is used for computation in the vertical. The formal discretizations of equations follows those described by Johns[4] and are not repeated here. It is, however, worthwhile to repeat the method of implementing equations (18) and (19), as this is crucial to the solution procedure.

A conventional subscript notation to reference grid point values of the dependent variable and a superscript to denote the time level are used. In practice we apply equation (19) at $x = L - \Delta x$, which is a u-point. Furthermore, we evaluate the depth-averaged velocity at the lower time level, thus introducing an error $O(\Delta t)$. This is consistent with the formal truncation error already present in our implicit evaluation of the vertical diffusion terms. Therefore we write equation (19) as

$$\bar{u}^p_{m-1} - \frac{1}{2}\left(\frac{g}{h_{m-1}}\right)^{1/2}(\zeta^{p+1}_m + \zeta^{p+1}_{m-2}) = -2u_L \sin(\sigma t). \tag{34}$$

Since ζ is not computed at $i = m - 1$, the value of it is replaced by the average of its values at the two adjacent ζ-points. Then equation (34) leads to

$$\zeta_m^{p+1} = -\zeta_{m-2}^{p+1} + 2\left(\frac{h_{m-1}}{g}\right)^{1/2} [2u_L \sin(\sigma t) + \bar{u}_{m-1}^p]. \tag{35}$$

Thus equation (35) yields a method of updating ζ at $x = L$ which utilizes an already known interior updated value of ζ together with the depth-averaged velocity derived from the previous time step.

Similarly, equation (18) leads to

$$\zeta_1^{p+1} = -\zeta_3^{p+1} + \left(\frac{h_2}{g}\right)^{1/2} (2u_0 - \bar{u}_2^p). \tag{36}$$

The method of implementation of equation (36) is similar to that of the above condition (35), except that it is applied at $x = \Delta x$ which is a u-point.

It is crucial that the finite difference analogue of equations (27) and (28) be correctly formulated and thus be compatible with equation (20). In order to achieve this, we use a discretization of the horizontal advection term in equations (27) and (28) based on one described by Roache.[5] This involves the application of a scheme of upstream differencing appropriate to a reversing flow and at the same time global conservation. Consequently, we obtain a strict fulfilment of the necessary requirement that any change in the total salinity and temperature in the estuary be balanced by the advective fluxes of salinity and temperature across $x = 0$ and $x = L$ (the diffusive fluxes of salinity and temperature across the end points of the estuary are dropped from the formulation).

The treatment of all terms in equation (28) is analogous to that of the corresponding terms in equation (25). Therefore we simply describe the basic form of the solution process to be applied to

$$\frac{\partial \tilde{S}}{\partial t} + \frac{\partial}{\partial x}(\tilde{u}S) = \mathscr{L}, \tag{37}$$

where $\mathscr{L}$ incorporates the effects of vertical advection and vertical diffusion.

The finite difference descritization of equation (37) has the form

$$\begin{aligned}\frac{\tilde{S}_{i,j}^{p+1} - \tilde{S}_{i,j}^p}{\Delta t} + \frac{1}{4\Delta x}[&(\tilde{u}_{i+1,j}^p - |\tilde{u}_{i+1,j}^p|)S_{i+2,j}^p + (\tilde{u}_{i+1,j}^p + |\tilde{u}_{i+1,j}^p| - \tilde{u}_{i-1,j}^p + |\tilde{u}_{i-1,j}^p|)S_{i,j}^p \\ &+ (-\tilde{u}_{i-1,j}^p - |\tilde{u}_{i-1,j}^p|)S_{i-2,j}^p] = \mathscr{L}_{i,j},\end{aligned} \tag{38}$$

where the terms in $\mathscr{L}_{i,j}$ are evaluated partly implicitly and partly explicitly.

Analysis of equation (38) reveals that the horizontal advection scheme has a required upstream property that guarantees the positivity of computed values of $\tilde{S}$. When applied at $i = 1$ with $\tilde{u}_{0,j}^p > 0, S_{-1,j}^p$ must be prescribed and is taken to be S_0, in which case equation (38) determines $\tilde{S}_{i,j}^{p+1}$. This situation corresponds to inflow at $x = 0$; $\tilde{S}_{i,j}^p$ can be determined from equation (38) without reference to $S_{-i,j}^p$. The only procedural problem is the determination of $\tilde{u}_{0,j}^p$, which is not deducible from the updating of the velocity distribution, because this is only carried out for $i = 2(2)m - 1$. Accordingly we have simply taken

$$\tilde{u}_{0,j}^p = \tilde{u}_{2,j}^p, \tag{39}$$

which represents a simple extrapolation of the computed velocity from the estuary. Therefore the computed dynamics of the estuarian model will imply whether a condition of inflow or outflow exists at $x = 0$ and equation (38) will then determine the corresponding local salinity conditions.

Similar comments may be made concerning the application of equation (38) for $i = m$. In this case

we have to assume

$$\tilde{u}^p_{m+1,j} = \tilde{u}^p_{m-1,j}. \tag{40}$$

Similar arguments can also be drawn for equation (27) when it is written in finite difference form. In the experiments we integrate the governing equations forward in time and with steady state forcing, continuing until the initial transient response is both radiated out of the analysis area and essentially dissipated by the action of friction. The remaining steady state fields will then represent the response to the prescribed steady state forcing.

NUMERICAL EXPERIMENTS

The Godavari Estuary (Figure 1) is modelled by taking $L = 26$ km of the main channel of the estuary neglecting its tributaries. The breadth and mean depth are based upon topographical and bathymetric information documented by Rao *et al.*[3] Thus over the length of the model estuary the breadth (taken as that of the central deep water channel) varies between 500 and 860 m and the mean depth varies between about 10 and 16 m. Results from two numerical experiments are described in this section that correspond to the freshwater flow conditions in the Godavari Estuary during the months of July and January. In both experiments the turbulent mixing parameters β and γ appearing in equations (12)–(14) are set equal to optimal values of 23 and 2·4 respectively; the reference depth h_0 is set equal to 16 m. The roughness length z_0 is set equal to 1 cm and, in accordance with the values used by Johns,[4] the empirical constant c is taken to be 0·08. With 29 computational points in the horizontal, the grid increment Δx has a value of about 930 m.

For the freshwater flow conditions during July we apply temperature and salinity boundary conditions (based on observations[3]) corresponding to $T_0 = 26{\cdot}5$ °C, $T_L = 27{\cdot}5$ °C, $S_0 = 0$ and $S_L = 34{\cdot}3$ ppt. The freshwater and tidal flow conditions in the estuary are fixed by taking $u_0 = 0{\cdot}047$ m s^{-1} and $u_L = 0{\cdot}4$ m s^{-1}. In order to ensure that our choice for the numerical value of u_L leads to the correct amplitude of the vertical components of the semi-diurnal tide, we have performed a Fourier analysis of the surface elevation ζ in the form

$$\zeta = \langle\zeta\rangle + \sum_k a_k \cos(k\sigma t - \phi_k), \tag{41}$$

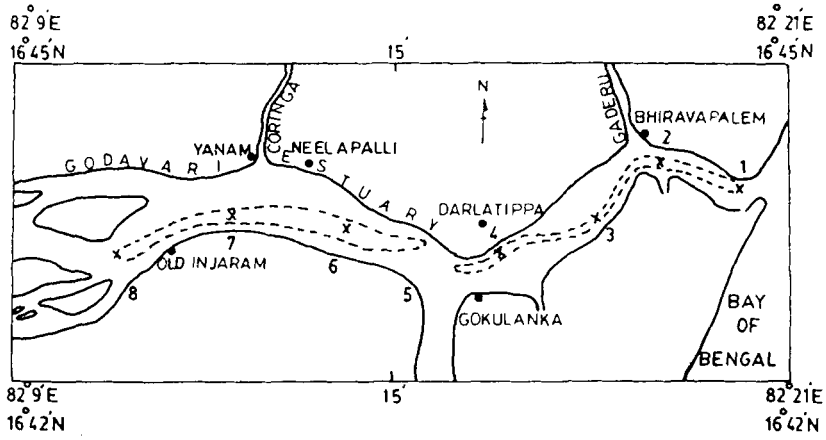

Figure 1. Godavari Estuary with station locations. Broken lines represent appropriate limits of deep water areas

where a_k and σ_k are the amplitude and phase angle of the kth harmonic respectively and $\langle\zeta\rangle$ is the mean value of the tidal elevation above equilibrium level. The principal interest here is in the value of the amplitude a_1 of the primary harmonic. With a parameter setting appropriate to the high-discharge conditions prevailing in July, we find that a_1 varies between about 0·41 m at $x = 0$ and 0·44 m at $x = L$. We also find that $\phi_1 = 124°$ at $x = 0$ and $\phi_1 = 99°$ at $x = L$, indicating that the phase of the tide takes about 51 min to propagate the 26 km comprising the length of the model estuary. Thus at all positions along the model estuary the time of occurrence of high (or low) water never differs by more than about 50 min. This is especially important, since the documented form of the observational data[3] implies that high (or low) tide occurs simultaneously at all positions along the estuary.

We show in Figure 2 the computed isolines of the salinity S, in parts per thousand (ppt), which correspond to the high-water phase of the tidal response. During this phase it will be noted that near-surface salt water has intruded more than 20 km along the estuary, producing salinities near $x = 0$ of the order of 4 ppt. This is in spite of a relatively strong seaward flow of near-surface fresh water which tends to oppose the inland penetration of saline water. It will be noted from Figure 2 that at a fixed section of the model estuary a surface layer having a depth of about 5 m tends to be well mixed, with the exception of the region corresponding to $9 < x < 19$ km. The existence of this feature appears to be related to the local occurrence of a marked reduction in the depth of water near $x = 16$ km. Below a depth of 5 m we note that at a fixed cross-section in the channel the conditions are again well mixed, with water having a salinity of 12 ppt having penetrated as far as the landward extremity of the model estuary. The transition between the surface and the lower layer is characterized by a level at which there is a locally sharp curvature in the isohalines. This divides the associated flow field into two distinct regions, which are most effectively illustrated by delineating the corresponding velocity profiles in Figure 3. From this figure it will be noted that during the peak high-water phase a freshwater surface outflow is accommodated in a layer having a thickness not exceeding 3 m. The predicted existence of a strong surface outflow layer during the high-water phase may appear to contradict the view expressed by Rao *et al.*[3] who imply that the associated flood tidal currents are directed landward at all depths. However, they do not point out that the peak flow currents at the surface persist for only a short time and that for most of the high-water phase the surface currents are eitehr very weak or actually in the

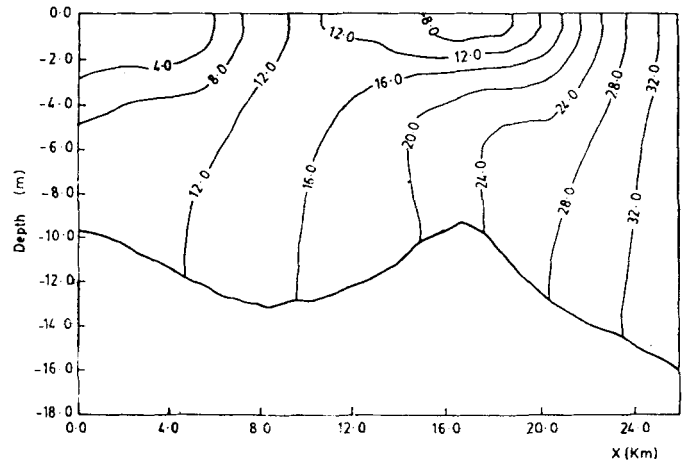

Figure 2. Computed salinity structure in July during the peak flood tide phase. The numbers on the contours refer to the salinity in parts per thousand

opposite direction. In our computations the peak flood tidal currents are confined to below a depth of about 3 m and attain their maximum values of about 0·6 m s^{-1} in the mid-depths of the estuary. Thus, given a persistent seaward near-surface flow during the high-water phase, the corresponding well-mixed saline conditions must be due to a dynamical exchange with the lower and more saline layers.

A similar analysis of the salinity distribution during the low-water or peak ebb phase of the tidal flow is shown in Figure 4. Here the combined strength of the ebb tidal and freshwater flow is seen to reduce the near-surface salinity to less than 4 ppt within about 15 km of the landward extremity of the estuary. Nearer the bed, water having a salinity of 12 ppt intrudes only to within 10 km of the landward limit. Compared with the flood tide case, it is also noteworthy that markedly reduced salinities are encountered near the mouth of the estuary as salt water flows into the open sea as a result of the strong surface seaward-directed currents existing during the peak ebb flow. This contrasts with the lower layers where salinities of the order of 26 ppt are encountered near the bed of the estuary. Accordingly, even during the ebb flow phase there appears to be an implied lower-layer inflow of water from the bay at the mouth of the estuary.

The velocity profiles during the peak ebb phase are shown in Figure 5. These clearly indicate the presence of a strong surface outflow of water with current speeds in excess of 1·1 m s^{-1}. In the lower layers of the flow, however, the currents are directed landward and attain speeds of the order of 0·5 m s^{-1}, thus explaining the occurrence of relatively high-salinity water at these levels. Hence throughout the tidal cycle the currents in the lower layer are exclusively landward, a condition supported by the baroclinic contribution to the horizontal pressure gradient and which results from the longitudinal salinity gradient.

In Figures 6(a) and 6(b) we reproduce the observed salinity structure during July as documented by Rao *et al.*[3] Figure 6(a) refers to the peak flood flow situation in which high-salinity water penetrates to the landward extremityy of the estuary. Except for the isolated surface salinity feature predicted in the mid-estuary region, the overall form of the observed isohalines agrees reasonably with the computed structure shown in Figure 2. Admittedly, the computed 12 and 16 ppt isohalines do intersect the bed of the estuary downstream of its landward extremity whereas they should continue horizontally upstream of $x = 0$. Nevertheless, the computed 24 ppt isohaline intersects the estuary bed in approximately the correct longitudinal position, the agreement with the observed structure improving markedly near the point of communication with the bay.

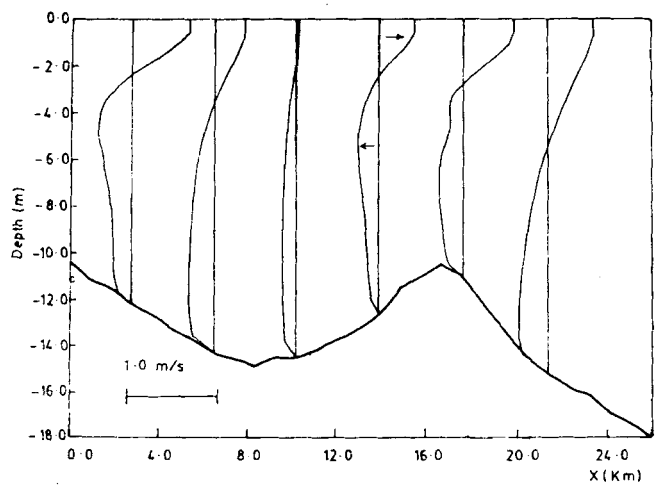

Figure 3. Computed velocity profiles in July during the peak flood tide phase

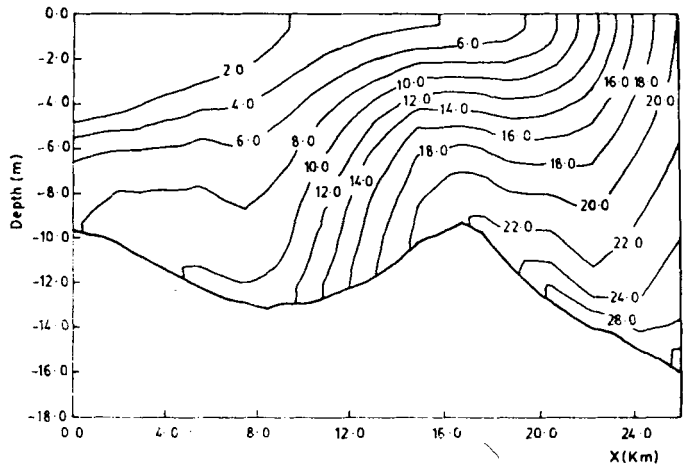

Figure 4. As Figure 2, but during the peak ebb tide phase

Figure 6(b) refers to the ebb flow phase in which the seaward flow in the surface layers strongly inhibits the inland penetration of surface saline water. Here the agreement of the computed isohaline structure with the observed form again appears resonably satisfactory, especially in connection with the prediction of low-salinity surface water within 15 km of the landward extremity of the estuary. It must, however, be pointed out that the computed salinity fields compare more favourably with their observational counterparts during the ebb tide phase than during the flood phase.

Given the composite nature of the fields shown in Figure 6, the overall quality of the comparison of the computed fields with observations suggests that it is worthwhile to evaluate the main features of the tidally averaged or mean density-controlled circulation. In this connection we delineate in Figure 7 the computed distribution of the mean isohalines in the estuary. This pattern shows a reduction in both the surface and near-bed salinity of more than 20 ppt over the length of the estuary. This pattern shows a reduction in both the surface and near bed salinity of more than 20 ppt over the length of the estuary.

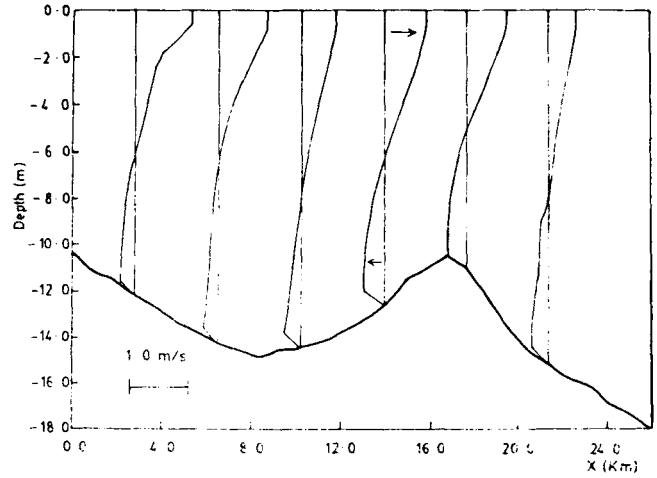

Figure 5. As Figure 3, but during the peak ebb tide phase

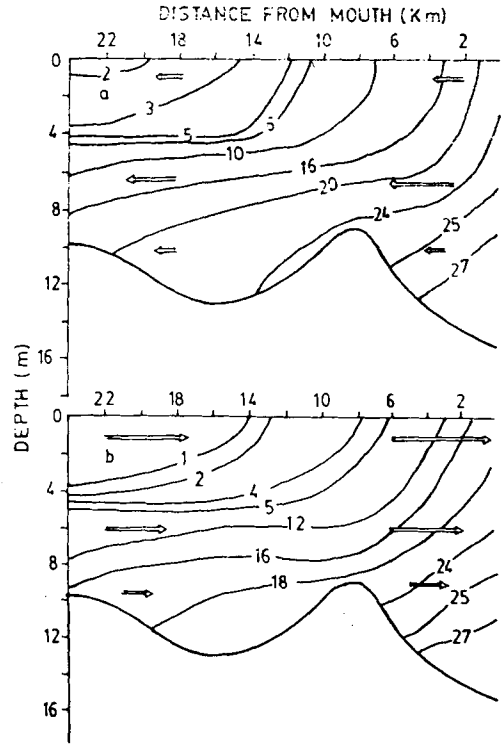

Figure 6. Observations of the salinity structure in July: (a) peak flood tide phase; (b) peak ebb tide phase. The numbers on the contours refer to the salinity in parts per thousand

At a fixed longitudinal position the outflow of freshwater has led to markedly reduced surface salinities in comparison with those at greater depths. This effect introduces a significant baroclinic component into the tidally averaged horizontal pressure gradient and induce a complex mean circulatory system in the estuary.

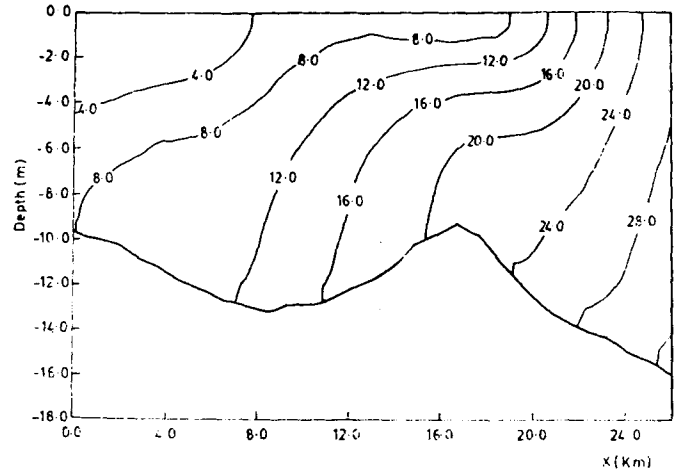

Figure 7. Computed mean salinity structure in July

An instantaneous streamfunction ψ for the volume transport may be defined as

$$bu = -\frac{\partial \psi}{\partial z}, \qquad bw = \frac{\partial \psi}{\partial x}, \tag{42}$$

where $\psi = 0$ at $z = -h$. Thus the instantaneous volume flux in the estuary is given by the value of $-(\psi)_{z=\zeta}$. The contours corresponding to constant values of $\langle\psi\rangle$ are shown in Figure 8. In this figure the bed of the estuary again corresponds to $\langle\psi\rangle = 0$. The mean volume flux in the estuary is given by the value of $-\langle(\psi)_{z=\zeta}\rangle$, which, consistently with our previous calculation, yields a net mean seaward transport of water amounting to 100 m^3 s^{-1}. Nevertheless, in the surface layer there is a predicted mean seaward volume transport of the order of 640 m^3 s^{-1}. Beneath the surface layer we note that there is a layer having a thickness of about 4 m in which there is no net mean transport of water. This region is characterized by the predicted existence of a closed mean circulation cell whose centre is located about 10 km from the mouth of the estuary. Farther upstream of this position the model circulations reveal the presence of a second circulation cell whose extent is only partly included in the present analysis area. These cells and the associated dynamical processes will evidently play a prominent role in the transfer of water properties between the near-surface and bottom layers of the flow field. Beneath this entrainment layer, we note the presence of a landward-directed mean flow in which there is a volume transport of the order of 640 m^3 s^{-1}. The net through volume transport of 100 m^3 s^{-1} (in our calculation of which we have taken account of the variation in the position of the free surface during the tidal cycle) is the difference between the much larger, oppositely directed mean volume transports in the surface and bottom layers.

The second experiment described here relates to the river flow during January when there is a negligible freshwater discharge. Tidal and freshwater flow conditions are fixed by choosing $u_0 = 0{\cdot}014$ m s^{-1} and $u_L = 0{\cdot}4$ m s^{-1}. Accordingly, with a reduced value of u_0 there will be an increased inland penetration of saline water from the bay and for a model estuary with a fixed length of 26 km there must be a change in the boundary conditions on S at $x = 0$ consistent with this fact. With this in mind we therefore choose $S_0 = 10$ ppt in contrast with $S_0 = 0$ in the previous experiment. All other temperature and salinity parameters remain unchanged. With this parameter setting, the mean volume flux through the estuary is found to be about 7 m^3 s^{-1}, a value consistent with the negligible discharge during January reported by Rao *et al.*[3]

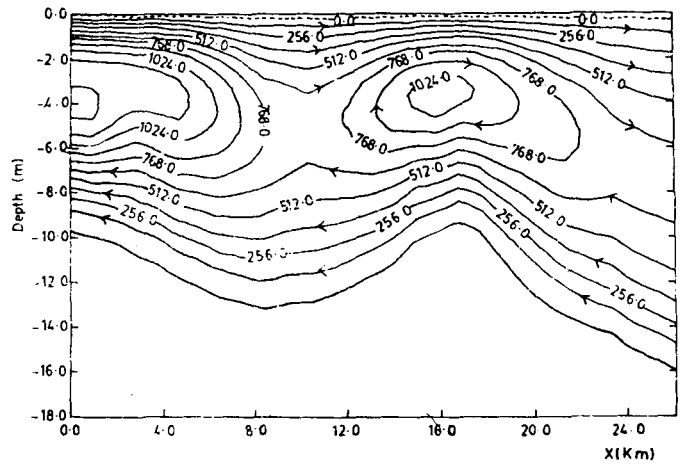

Figure 8. Computed mean volume transport streamlines in July. The numbers on the contours refer to the volume transport rate in m^3 s^{-1}

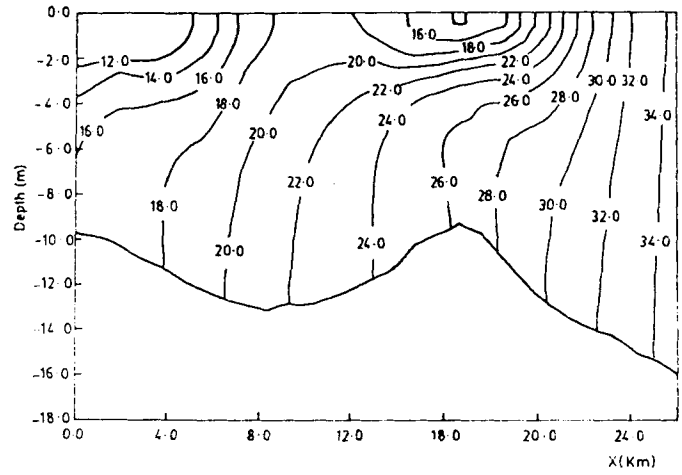

Figure 9. As Figure 2, but in January

In Figure 9 we show the isolines of S that correspond to the high-water phase of the tidal flow. During this flood period it will be noted that there is a predicted penetration of surface water with a salinity of 18 ppt to within 8 km of the landward extremity of the estuary. At a fixed longitudinal position the surface and bottom layers tend to be well mixed, with bottom water having a salinity of 21 ppt penetrating to within 8 km of the landward extremity of the estuary. At this phase of the tide there is again an isolated surface feature at about 10 km from the mouth of the estuary characterized by a local minimum in the salinity of less than 14 ppt. In Figure 10 we show the salinity structure during the flow tide phase when the currents have their maximum ebb values. In comparison with the flood tide case, when the maximum salinity in the estuary is 34 ppt, the maximum value has now been reduced to 30 ppt, this being a consequence of the reduced input of salt from the bay. The measured salinity structure based upon the observations[3] is shown in Figures 11(a) and 11(b). A comparison with

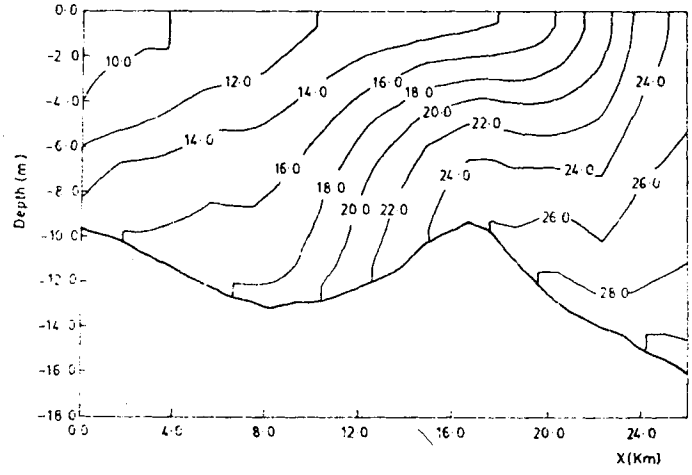

Figure 10. As Figure 4, but in January

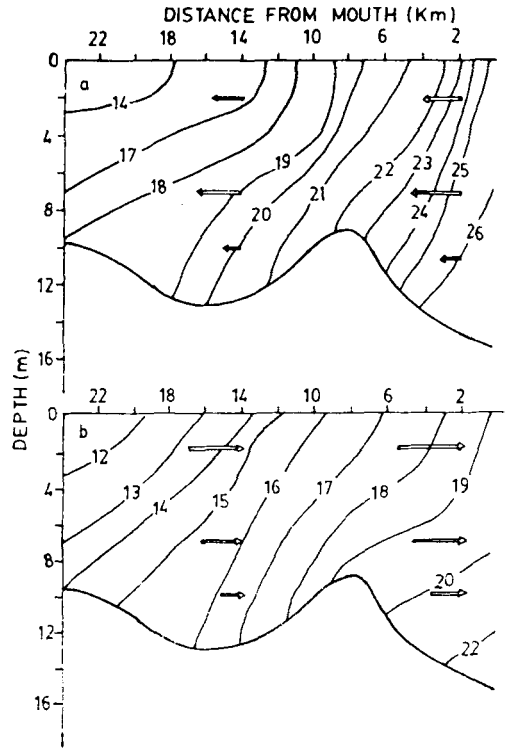

Figure 11. As Figure 6, but in January

the corresponding computed structures depicted in Figures 9 and 10 indicates a satisfactory overall agreement. The other dynamical and salinity features for January are qualitatively similar to those prescribed for July.

CONCLUSIONS

Numerical experiments have been performed to simulate the tidal and salinity structure in the Godavari Estuary. Using a multilevel numerical model, tidal and turbulent mixing parameters have been chosen so as to yield the best overall agreement with observational data.[3] With the corresponding parameter setting, an anlaysis has been made of the computed mean circulation in the estuary during seasons of both high and low freshwater discharge.

REFERENCES

1. K. R. Dyer, *Estuaries: A Physical Introduction*, Wiley, London, 1973.
2. C. B. Officer, *Physical Oceanography of Estuaries (and Associated Coastal Waters)*, Wiley, New York, 1976.
3. V. R. Rao, Y. V. Ramana and B. S. R. Reddy, 'Salinity and current distribution in the Godavari Estuary, east coast of India', *Indian J. Marine Sci.*, **17**, 14–18 (1988).
4. B. Johns, 'The modelling of tidal flow in a channel using a turbulence energy scheme', *J. Phys. Oceanogr.*, **8**, 1042–1049 (1978).
5. P. J. Roache, *Computer Fluid Dynamics*, Hermosa, Albuquerque, NM, 1972.